

# Exact eddy-viscosity equation for turbulent wall flows

Emmanuel Plaut<sup>1</sup> & Stefan Heinz<sup>2</sup>

<sup>1</sup>Université de Lorraine, CNRS, LEMTA, F-54000 Nancy, France

<sup>2</sup>Mathematics Department, University of Wyoming, Laramie, WY, USA

Confidential draft **PlautHeinz20.pdf** - Version 0.085 of June 4, 2020

## Table of contents

<b>Please check the <i>What's new</i> section at the end of this table !</b>	<b>1</b>
<b>Abstract</b>	<b>2</b>
<b>1 Introduction</b>	<b>2</b>
<b>2 Flow cases and state of the art</b>	<b>2</b>
2.1 Turbulent wall flows . . . . .	2
2.2 RANS models with an eddy-viscosity equation . . . . .	2
2.3 The Scale - Adaptive Simulation models . . . . .	3
2.4 Analytic eddy viscosity model of turbulent wall flows . . . . .	4
<b>3 Analysis: exact eddy-viscosity equation</b>	<b>5</b>
3.1 Generalities . . . . .	5
3.2 Application to channel flows . . . . .	7
3.3 Application to pipe flows . . . . .	7
3.4 Application to boundary layers . . . . .	7
3.5 Asymptotic structure of the near-wall dissipation . . . . .	11
3.6 Asymptotic structure of the production . . . . .	12
3.7 Asymptotic structure of the outer dissipation . . . . .	12
3.8 QR6 on the BL case inspired from Spalart & Allmaras (1994) . . . . .	13
<b>References</b>	<b>14</b>
<b>Please check the <i>Archives</i> section at the end of this document !</b>	<b>14</b>
<b>What's new in this Version 0.085 of June 4, 2020</b>	

- I concluded the section 3.8 around my Q6.

## Abstract

A recent theory has been developed (Heinz 2018, 2019) for three canonical turbulent wall flows: channel flow, pipe flow and zero-pressure gradient boundary layer, that offers exact analytical formulas for the RANS eddy-viscosity. By calculating the eddy-viscosity turbulent diffusion term for these flows where the turbulence is stationary, one identifies a high-Reynolds number RANS eddy-viscosity equation with one production and two dissipation terms. One dissipation term is universal and peaks in the near-wall region. The second one, smaller in magnitude, is flow-dependent and peaks in the wake region. The production term is flow-dependent and peaks in between. The universal dissipation term implies a damping function and a length scale analogous to the von Karman length scale used in the Scale-Adaptative Simulation models. This length scale also appears in the production term. This confirms on firm theoretical bases the relevance of von Karman length scales. This is an occasion to analyze these length scales in more details. An asymptotic analysis of the eddy-viscosity budget in the limit of infinite Reynolds numbers is also proposed. This allows a review and tests of existing RANS models that imply an eddy-viscosity equation. Finally, we propose a new version of the eddy-viscosity equation of the Scale-Adaptative Simulation models.

## 1 Introduction

*To be written !..*

## 2 Flow cases and state of the art

### 2.1 Turbulent wall flows

*A part of the text below, especially of the first sentences, will probably move to the introduction...*

Wall-bounded turbulent flows are ubiquitous in human-made fluid systems, and are also encountered in the nature: the atmospheric boundary layer for instance is the place where we live and where we like to set up buildings, wind turbines, etc. In the infinite family of these flows, one may distinguish three canonical cases: channel flow, pipe flow and the zero-pressure gradient turbulent boundary layer, or ‘boundary layer’, for the sake of concision. These flows, denoted here ‘turbulent wall flows’, are somewhat simpler, because the geometry of the fluid domain is simple and highly symmetric, but they still present a good richness of behaviour. We will build an exact eddy-viscosity equation for these three cases, and discuss the possible consequences on other classical models. Before presenting those, let us fix the hypotheses and notations. We consider an incompressible fluid of mass density  $\rho$  and kinematic viscosity  $\nu$ . In wall-bounded turbulent flows in general, locally a cartesian system of coordinates  $Oxyz$  is used, such that  $x$  points in the streamwise direction, and  $y$  measures the distance to the closest wall. To lowest order, the mean flow

$$\mathbf{U} = U(y, t) \mathbf{e}_x \quad (1)$$

where  $\mathbf{e}_x$  is the unit vector in the  $x$ -direction,  $t$  time. A relevant quantity is the mean strain rate

$$S = \partial U / \partial y, \quad (2)$$

which may be evaluated in more general three-dimensional flows from the full strain-rate tensor, see e.g. the equation (20) of Menter (1997). Focusing now onto the canonical turbulent wall flows, the length scale  $\delta$  is the half-channel height, pipe radius, or 99% boundary layer thickness with respect to channel flow, pipe flow, and boundary layer, respectively. Denoting  $u_x \mathbf{e}_x + u_y \mathbf{e}_y + u_z \mathbf{e}_z$  the fluctuating velocity, the RANS eddy viscosity

$$\nu_t = - \langle u_x u_y \rangle / S \quad (3)$$

where the angular brackets denote the Reynolds average. The mean wall shear stress  $\tau_w$  is used to define the friction velocity  $u_\tau = \sqrt{\tau_w / \rho}$ . From this are defined wall or inner units, i.e.  $y^+ = u_\tau y / \nu$ ,  $U^+ = U / u_\tau$  and

$$S^+ = \partial U^+ / \partial y^+. \quad (4)$$

Finally, the friction-velocity Reynolds number  $Re_\tau = \delta^+ = u_\tau \delta / \nu$ .

### 2.2 RANS models with an eddy-viscosity equation

*To be written, by citing at least Nee & Kovaszny (1969); Baldwin & Barth (1990); Spalart & Allmaras (1994); Menter (1997); Yoshizawa et al. (2012) ...*

## 2.3 The Scale - Adaptive Simulation models

*To be written, by citing at least Menter & Egorov (2006, 2010); Egorov et al. (2010); Abdol-Hamid (2015) !.. Following Menter & Egorov (2010), introduce in particular their turbulent length-scale*

$$\ell_t = C_\mu^{-1/4} k^{-1/2} \nu_t, \quad (5)$$

the von Karman length-scale

$$\ell_{vK} = \kappa \left| \frac{S}{\partial S / \partial y} \right|, \quad (6)$$

with  $\kappa$  the von Karman constant, and their eddy-viscosity equation

$$\frac{\partial \nu_t}{\partial t} = \frac{1}{\sigma_M} \frac{\partial}{\partial y} \left( \nu_t \frac{\partial \nu_t}{\partial y} \right) + P_{\nu M} - D_{\nu M} \quad (7)$$

with

$$P_{\nu M} = \zeta_1 \frac{\nu_t^2 S^2}{k}, \quad (8a)$$

$$D_{\nu M} = \zeta_2 \frac{\nu_t^2 S^2}{k} \left( \frac{\ell_t}{\ell_{vK}} \right)^2 + C_\mu^{1/4} \zeta_3 k, \quad (8b)$$

$$(\sigma_M, \zeta_1, \zeta_2, \zeta_3) = (2/3, 0.8, 1.47, 0.0288). \quad (8c)$$

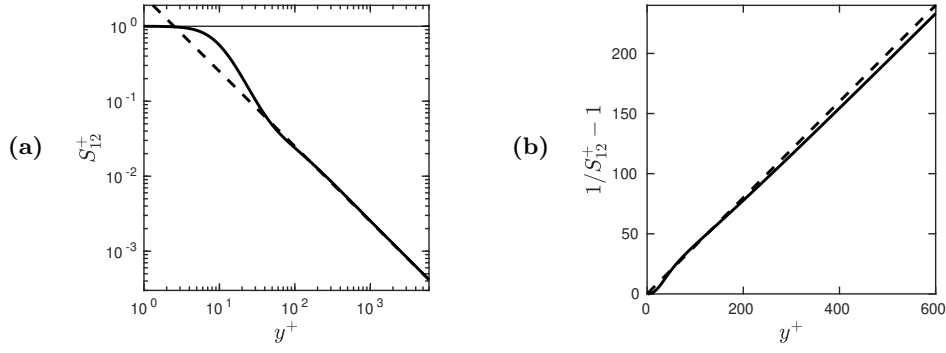


**Fig. 1** : (a) Continuous line:  $S_{12}^+$ , dashed line:  $1/(\kappa y^+)$ . (b) Continuous line:  $1/S_{12}^+ - 1$ , dashed line:  $\kappa y^+$ .

## 2.4 Analytic eddy viscosity model of turbulent wall flows

Heinz (2018, 2019) proposed analytic models for the mean flow  $U$ , main Reynolds stress  $-\langle u_x u_y \rangle$  and eddy viscosity  $\nu_t$  of the turbulent wall flows defined in section 2.1. In the equation (11) of Heinz (2019), an analytic expression is proposed for the reduced eddy viscosity, which is valid at high Reynolds number,  $Re_\tau \gtrsim 500$ ,

$$\nu^+ = \nu_t/\nu = (1/S_{12}^+ - 1) W. \quad (9)$$

There  $S_{12}^+ = S_1^+ + S_2^+$  is a very good approximation of the dimensionless mean strain rate  $S^+$  (4) in the inner region of the flows, i.e., disregarding wake effects, see the equation (7) of Heinz (2018) and the corresponding discussion. Precisely, the universal function

$$S_{12}^+ = S_{12}^+(y^+) = 1 - \left[ \frac{(y^+/a)^{b/c}}{1 + (y^+/a)^{b/c}} \right]^c + \frac{1}{\kappa y^+} \frac{1 + h_2/(1 + y^+/h_1)}{1 + y_k/(y^+H)}, \quad (10)$$

with

$$a = 9, \quad b = 3.04, \quad c = 1.4, \quad H = H(y^+) = (1 + h_1/y^+)^{-h_2}, \quad h_1 = 12.36, \quad h_2 = 6.47, \quad y_k = 75.8, \quad (11)$$

and the von Karman constant

$$\kappa = 0.40. \quad (12)$$

The function  $S_{12}^+$ , plotted on the figure 1a, approaches naturally 1 as  $y^+ \rightarrow 0$  in the viscous sublayer. On the contrary, as  $y^+ \rightarrow \infty$ ,  $S_{12}^+ \sim 1/(\kappa y^+)$ , in agreement with the log law. Therefore the function  $1/S_{12}^+ - 1$ , plotted on the figure 1b, which appears in the eddy viscosity (9), vanishes in the limit  $y^+ \rightarrow 0$ , and then increases smoothly to approach the function  $\kappa y^+$  as  $y^+ \rightarrow \infty$ .

The second ingredient of the theory is the function  $W$ , which is flow-dependent and in outer scaling, because it describes wake effects. With the notations of Heinz (2018, 2019),  $W = 1/G_{CP}$  for channel and pipe flows,  $M_{BL}/G_{BL}$  for boundary layers, where  $G_{CP}$  and  $G_{BL}$  characterize the wake contribution  $S_3^+$  to the dimensionless mean strain rate  $S^+$  (see the equations 7 and A.22 of Heinz 2018),  $M_{BL}$  characterizes the total stress in boundary layers (see the equation 4 of Heinz 2019). For channel and pipe flows

$$W = W_X(y/\delta) \quad \text{with} \quad W_X(y) = \frac{K_X y + (1 - y)^2(0.6y^2 + 1.1y + 1)}{1 + y + y^2(1.6 + 1.8y)}, \quad (13)$$

$X = C$ ,  $K_C = 0.933$  for channel,  $X = P$ ,  $K_P = 0.687$  for pipe; for boundary layers

$$W = W_{BL}(y/\delta) \quad \text{with} \quad W_{BL}(y) = \frac{1 + 0.285 y e^{y(0.9+y+1.09y^2)}}{1 + (0.9 + 2y + 3.27y^2)y} e^{-y^6 - 1.57y^2}. \quad (14)$$

The wake function  $W$  is plotted for these three flows on the figure 2a. In the near-wall region, when  $y/\delta \rightarrow 0$ ,  $W \rightarrow 1$ , hence the eddy viscosity (9),  $\nu^+ = (1/S_{12}^+(y^+) - 1) W(y^+/\delta^+) \sim (1/S_{12}^+(y^+) - 1)$  where  $\delta^+ = Re_\tau$ . Therefore the log-layer eddy viscosity  $\kappa y^+$  is approximately recovered if  $1 \ll y^+ \ll \delta^+$ ; for a more precise study, see the section 4.1 of Heinz (2019). When  $y$  becomes of the order of  $\delta$ , wake effects come in, that saturate the growth of the eddy viscosity (9), since  $W$  decreases. Whereas the maximum value of  $y$  is  $\delta$  in channel and pipe flows (in channel flow if  $y \in [\delta, 2\delta]$  the mean fields can be obtained by suitable symmetries from the mean fields for  $y \in [0, \delta]$ ), it may be much larger in boundary layers. Naturally,  $W_{BL} \rightarrow 0$  as  $y \rightarrow \infty$ ; precisely  $W_{BL} < 10^{-3}$  as soon as  $y > 1.36\delta$ .

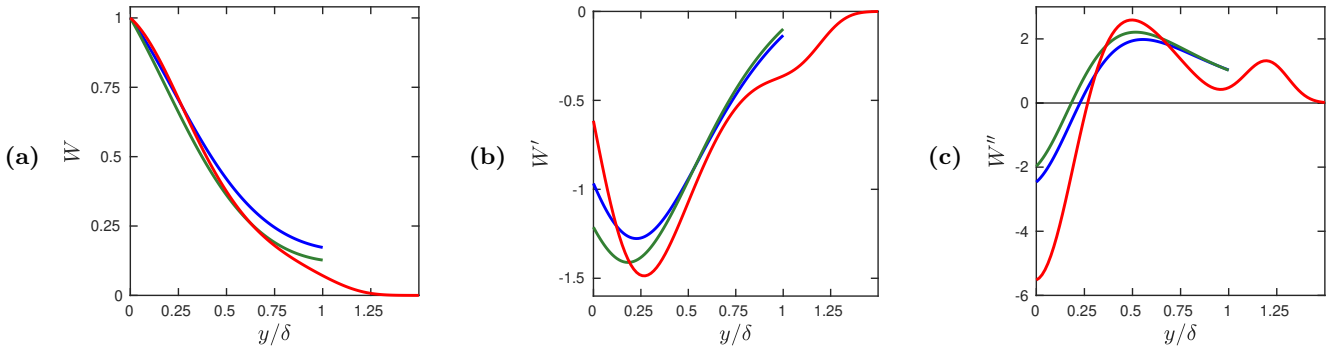


**Fig. 2 :** (a)  $W$  (b)  $W'$  (c)  $W''$  for channel (blue), pipe (green), boundary layer (red).

The theory of Heinz (2018, 2019) has been validated by a thorough study of DNS data, including those of Lee & Moser (2015); Chin *et al.* (2014); Sillero *et al.* (2013), and experimental data, for instance those of Vallikivi *et al.* (2015). For instance, the figures S.6abc of the supplementary material to Heinz (2019) show the eddy viscosity of various DNS, one for each canonical flow, compared with two variants of the eddy-viscosity model (9). In particular, the magenta curves show  $\kappa y^+ W$  with our notations, i.e.  $(1/S_{12}^+ - 1)$  in (9) has been replaced by  $\kappa y^+$ . The agreement with the DNS is good, except in the outer region, where in (3) both the numerator  $\langle u_x u_y \rangle$  and the denominator  $dU/dy$  tend to zero, hence the DNS noise is amplified.

Since the derivatives  $W'$  and  $W''$  will be needed hereafter, they are plotted on the figures 2bc. Whereas the functions  $W$  for the three flow cases are quite similar (figure 2a), their first and second derivatives show larger differences (figures 2bc). Naturally,  $W'_{BL}$  and  $W''_{BL} \rightarrow 0$  as  $y \rightarrow \infty$ .

### 3 Analysis: exact eddy-viscosity equation

#### 3.1 Generalities

Since the focus of our study is on high-Reynolds numbers wall-bounded flows, we assume that the form of the eddy-viscosity equation is

$$\sigma \frac{\partial \nu_t}{\partial t} = \frac{\partial}{\partial y} \left( \nu_t \frac{\partial \nu_t}{\partial y} \right) + P_\nu - D_\nu \quad (15)$$

with  $y$  the wall distance,  $P_\nu > 0$  the production,  $D_\nu > 0$  the dissipation term. The dimensionless coefficient  $\sigma$ , of order 1, which is a kind of Prandtl number, plays no role in the canonical turbulent wall flows, where the mean fields are steady, but is kept in (15) for the sake of comparison with other turbulence models. In turbulent wall flows, according to (15), the opposite of the turbulent diffusion term

$$-T_\nu = -\frac{\partial}{\partial y} \left( \nu_t \frac{\partial \nu_t}{\partial y} \right) = P_\nu - D_\nu . \quad (16)$$

A formal computation of  $T_\nu$  starting from (9) leads to  $D_\nu = D_{\nu i} + D_{\nu o}$  and

$$D_{\nu i} = \kappa^2 \frac{\nu_t^2}{L_{vK}^2} \frac{1}{f^2} , \quad (17a)$$

$$P_\nu = \kappa \frac{\nu_t^2}{L_{vK} \delta} \frac{1}{1 - S_{12}^+} \left( -\frac{4W'}{W} \right) = \kappa \frac{\nu \nu_t}{L_{vK} \delta} \frac{1}{S_{12}^+} (-4W') , \quad (17b)$$

$$D_{\nu o} = \frac{\nu_t^2}{\delta^2} \frac{W'^2 + WW''}{W^2} = \frac{\nu^2}{\delta^2} (1/S_{12}^+ - 1)^2 (W'^2 + WW'') . \quad (17c)$$

The indices  $i$  and  $o$  refer to ‘inner’ and ‘outer’ terms, respectively, and the notation  $D_{\nu o}$  is slightly improper since this term is slightly negative in the near-wall region. However,  $D_{\nu o}$  is much smaller in this region than in the outer region where it peaks, as it will be shown in the figure 6b for channel flow, 7b for pipe flow, 8b for boundary layers. Moreover  $D_\nu = D_{\nu i} + D_{\nu o} > 0$  everywhere, as it will be shown in the figures 6cd for channel flow, 7cd for pipe flow, 8cd for boundary layers, hence the notation  $D_\nu$  is fully justified.

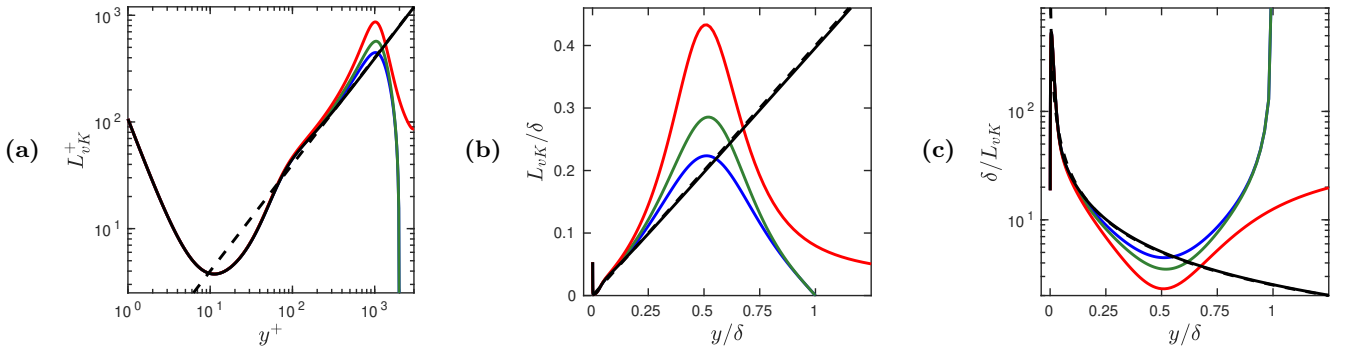


**Fig. 3 :** (a,b) The asymptotic von Karman length scale  $L_{vK}$  (18) (black continuous); its log law approximation  $\kappa y$  (black dashed); the von Karman length scale  $\ell_{vK}$  (6) for channel (blue), pipe (green), boundary layer (red). The  $\ell_{vK}^+$  curves of the figure (a) and all curves of the figure (b) have been computed at  $Re_\tau = 2000$ . All curves have been computed starting at  $y^+ = 1$ . The figure (c) shows the same curves as figure (b) but with the inverse ordinates and linear-log scales.

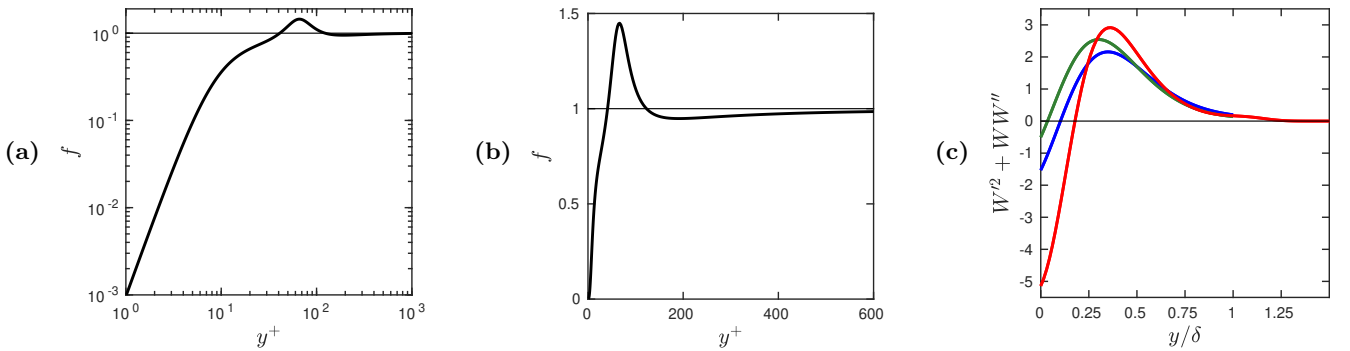


**Fig. 4 :** (a,b) The damping function  $f$ . (c) The function  $W'^2 + WW''$  for channel (blue), pipe (green), boundary layer (red).

In addition to the functions  $S_{12}^+$  and  $W$  defined in the section 2.4, there appears in the equations (17) other functions that are built on these. The first one is the asymptotic von Karman length scale

$$L_{vK} = \kappa \left| \frac{S_{12}}{\partial S_{12}/\partial y} \right| \quad \text{or} \quad L_{vK}^+ = \kappa \left| \frac{S_{12}^+}{\partial S_{12}^+/\partial y^+} \right|, \quad (18)$$

which is defined as the von Karman length scale  $\ell_{vK}$  (6), but replacing  $S$  by  $S_{12}$ , i.e., disregarding ‘wake effects’. The fact that the length scale  $L_{vK}$  appears in (17a) and (17b) confirms on very firm bases the relevance of this length scale, which was not so clear in the works of Rotta. Only the inner-units  $L_{vK}^+(y^+)$  is universal, whereas the physical  $L_{vK}(y/\delta)$  has to be calculated as  $\delta(L_{vK}^+/\delta^+)$ , i.e.  $L_{vK}/\delta$  depends on  $\delta^+ = Re_\tau$ . Since, as  $y^+ \rightarrow \infty$ , in agreement with the log law,  $S_{12}^+ \sim 1/(\kappa y^+)$ ,  $L_{vK}^+ \sim \kappa y^+$ , as confirmed by the figure 3a. The functions  $\ell_{vK}^+(y^+)$  (figure 3a) or  $\ell_{vK}(y/\delta)$  (figure 3b), that depend on the flow case and Reynolds-number, have been computed using the accurate expressions of  $S^+$  of the equation (7) of Heinz (2018). In channel or pipe flow,  $U$  presents a maximum at the centerplane or pipe axis  $y = \delta$ , hence  $S$  and  $\ell_{vK}$  vanish there. On the contrary, in boundary layer flow,  $S$  and  $\ell_{vK}$  vanish only in the limit  $y \rightarrow \infty$ . The figure 3c suggests that, because the dimensional factor in  $D_{\nu i}$  (17a),  $P_\nu$  (first expression in 17b) and  $D_{\nu o}$  (first expression in 17c) are respectively  $\nu_t^2/L_{vK}^2$ ,  $\nu_t^2/(L_{vK}\delta)$  and  $\nu_t^2/\delta^2$ , in the ratii  $\delta^2/L_{vK}^2$ ,  $\delta/L_{vK}$ , 1, those will peak in the inner, intermediate and outer regions; this will be confirmed in the figures 6 for channel flow, 7 for pipe flow, 8 for boundary layers.

Another ingredient in  $D_{\nu i}$  (17a), is the universal damping function

$$f = f(y^+) = (1 - S_{12}^+) \left( \frac{(S_{12}^+ - 1) S_{12}^+ d^2 S_{12}^+ / dy^{+2}}{(dS_{12}^+ / dy^+)^2} + 3 - 2S_{12}^+ \right)^{-1/2}. \quad (19)$$

It is plotted on the figures 4ab. It does tend to zero as  $y^+ \rightarrow 0$  and 1 as  $y^+ \rightarrow \infty$ .

Finally, in  $P_\nu$  (17b) and  $D_{\nu o}$  (17c) the rightmost functions depend only on  $W$  and its derivatives. In  $P_\nu$  there appears  $-4W'$  which is positive according to the figure 2b, hence  $P_\nu > 0$  as required. In  $D_{\nu o}$  there appears  $W'^2 + WW''$  which is plotted on the figure 4c. As already suggested at the level of (16,17), the function  $W'^2 + WW'' > 0$  except in a more or less narrow near-wall region, depending on the flow case.

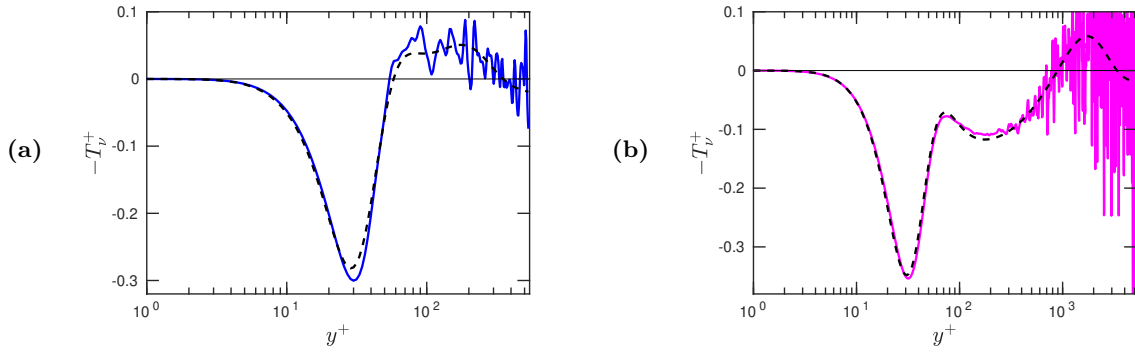


**Fig. 5** : The continuous line shows the opposite of the dimensionless turbulent diffusion term  $-T_\nu^+$  (20) computed with the channel flow DNS of Lee & Moser (2015) at  $Re_\tau = 543$  (a), 5186 (b). The dashed line shows the same term computed with our model (21).

### 3.2 Application to channel flows

In typical channel flow cases, a comparison of the opposite of the dimensionless turbulent diffusion term

$$-T_\nu^+ = -\frac{\partial}{\partial y^+} \left( \nu^+ \frac{\partial \nu^+}{\partial y^+} \right) \quad (20)$$

computed with finite differences from two DNS of Lee & Moser (2015) and its model (16,17),

$$-T_\nu^+ = P_\nu^+ - D_\nu^+ = -D_{\nu i}^+ + P_\nu^+ - D_{\nu o}^+ \quad (21)$$

is shown on the figures 5. Except in the outer region, where the DNS noise is amplified, there is a good agreement between the model and the DNS, especially, for the highest Reynolds number case.

The separation of  $-T_\nu^+$  into the three terms of the model,  $-D_{\nu i}^+$ ,  $P_\nu^+$  and  $-D_{\nu o}^+$ , is illustrated on the figures 6. The comparison of the figures 6a, c and g shows that the dissipation term  $D_{\nu i}^+$  dominates in the near-wall region. In this region, and in inner scalings,  $D_{\nu i}^+(y^+)$ ,  $D_\nu^+(y^+)$  and  $T_\nu^+(y^+)$  approach as  $Re_\tau \rightarrow \infty$  a limit profile, with a maximum around  $y^+ = 31$  and a minimum around  $y^+ = 72$ . A plateau around  $y^+ \simeq 300$  and

$$D_{\nu i}^+ \simeq D_\nu^+ \simeq T_\nu^+ \simeq \kappa^2$$

builds up as  $Re_\tau \rightarrow \infty$ , in agreement with the formula for the log-layer reduced eddy viscosity,  $\nu^+ = \kappa y^+$ . For larger values of  $y/\delta$ , after this plateau, the figures 6bdfh show that all terms, considered in inner-outer scalings,  $D_{\nu i}^+(y/\delta)$ ,  $D_{\nu o}^+(y/\delta)$ ,  $D_\nu^+(y/\delta)$ ,  $P_\nu^+(y/\delta)$  and  $T_\nu^+(y/\delta)$ , approach limit profiles as  $Re_\tau \rightarrow \infty$ .

### 3.3 Application to pipe flows

In the eddy-viscosity model (9), the only difference between channel and pipe flows is described by the change of the coefficient  $K_X$  in the function  $W_X$  (13) that contains the wake effects. This change from  $K_C = 0.933$  to  $K_P = 0.687$  is moderate, therefore the turbulent diffusion term and its contributions are close to the ones of channel flow, as shows the comparison between the figures 6 and figures 7. All the comments made on the figures 6 at the end of section 3.2 also apply to the figures 7.

### 3.4 Application to boundary layers

The boundary layer case differs from the channel and pipe flow cases in that the maximum value of  $y$  (resp.  $y^+$ ) is not  $\delta$  (resp.  $\delta^+ = Re_\tau$ ) but, in principle, infinity. Moreover, the wake function  $W$  of boundary layers (14) differs significantly from the one of channel and pipe flows (13). The comparison of the figures 8 with the figures 6 and 7 shows similar behaviours in the ranges  $y \in [0, \delta[$  i.e.  $y^+ \in [0, \delta^+[$ , whereas there are differences in the outer region. At  $y = \delta$ , i.e. the centerplane in channels or the pipe axis in pipes, the function  $T_\nu$  should present a vanishing slope for symmetry reasons, as confirmed by the figures 6h and 7h; note that the outer term  $-D_{\nu o}^+$  plays an important role there. In boundary layers, one does not expect a similar property, but that  $T_\nu$  should approach 0 as  $y \rightarrow \infty$ . This is what suggests the figure 8h, and what would confirm a figure drawn with a larger interval of the abscissas (not shown): for all the Reynolds numbers implied, that range from 543 to 30000,  $|T_\nu^+| < 10^{-3}$  as soon as  $y > 1.32\delta$ .

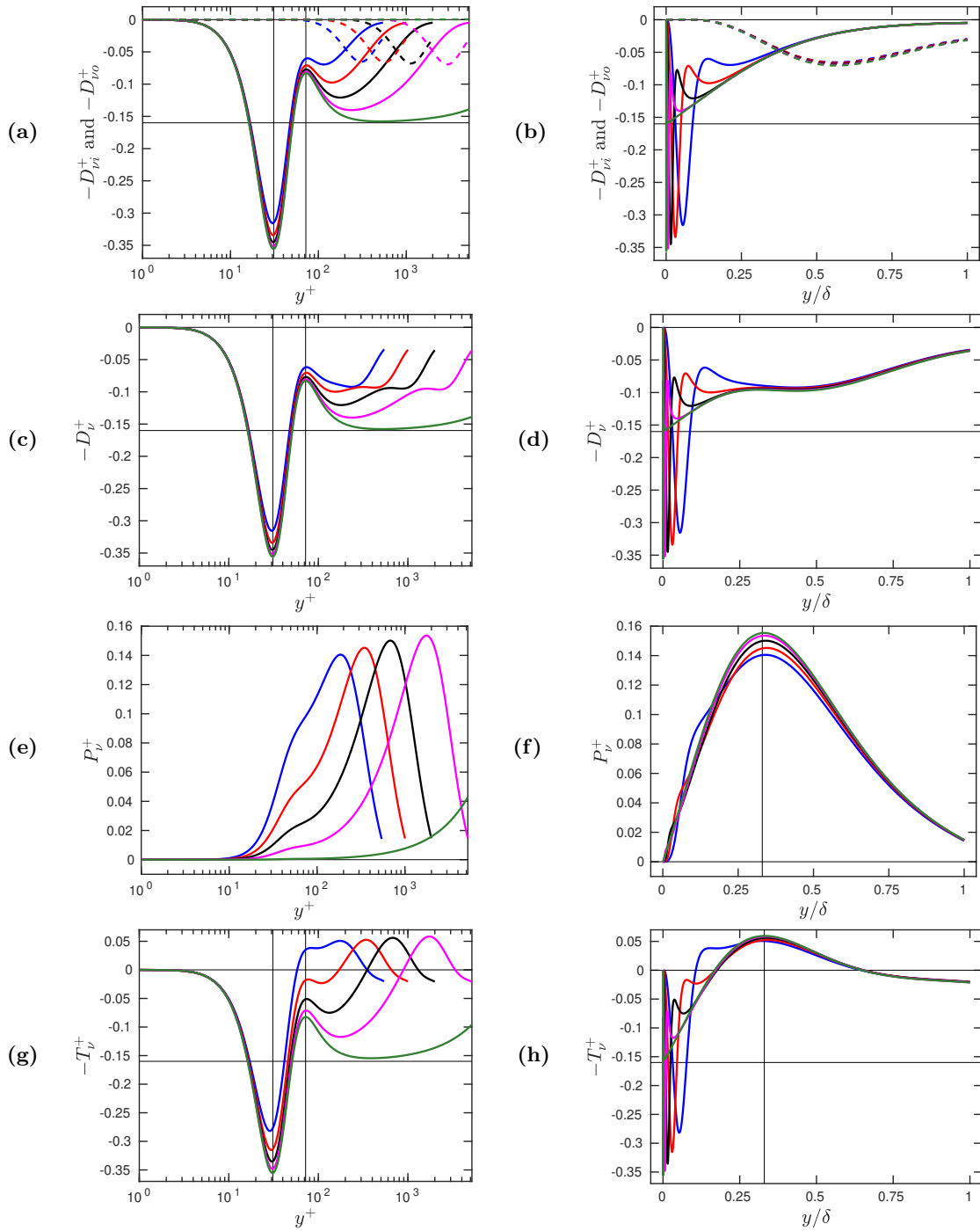


**Fig. 6** : For channel flows at  $Re_\tau = 543$  (blue), 1001 (red), 1995 (black), 5186 (magenta), 80000 (green), the various contributions to  $-T_v^+$  (21) and their sum. **(a,b)**  $-D_{v_i}^+$  with the continuous,  $-D_{v_o}^+$  with the dashed lines. **(c,d)**  $-D_v^+$ . **(e,f)**  $P_v^+$ . **(g,h)**  $-T_v^+$ . On **(a,c,g)** the vertical lines are at  $y^+ = 31$  and  $72$ ; on **(f,h)** they are at  $y = 0.33\delta$ . On **(a,b,c,d,g,h)** the horizontal lines are at  $-T_v^+ = 0$  and  $-\kappa^2$ .



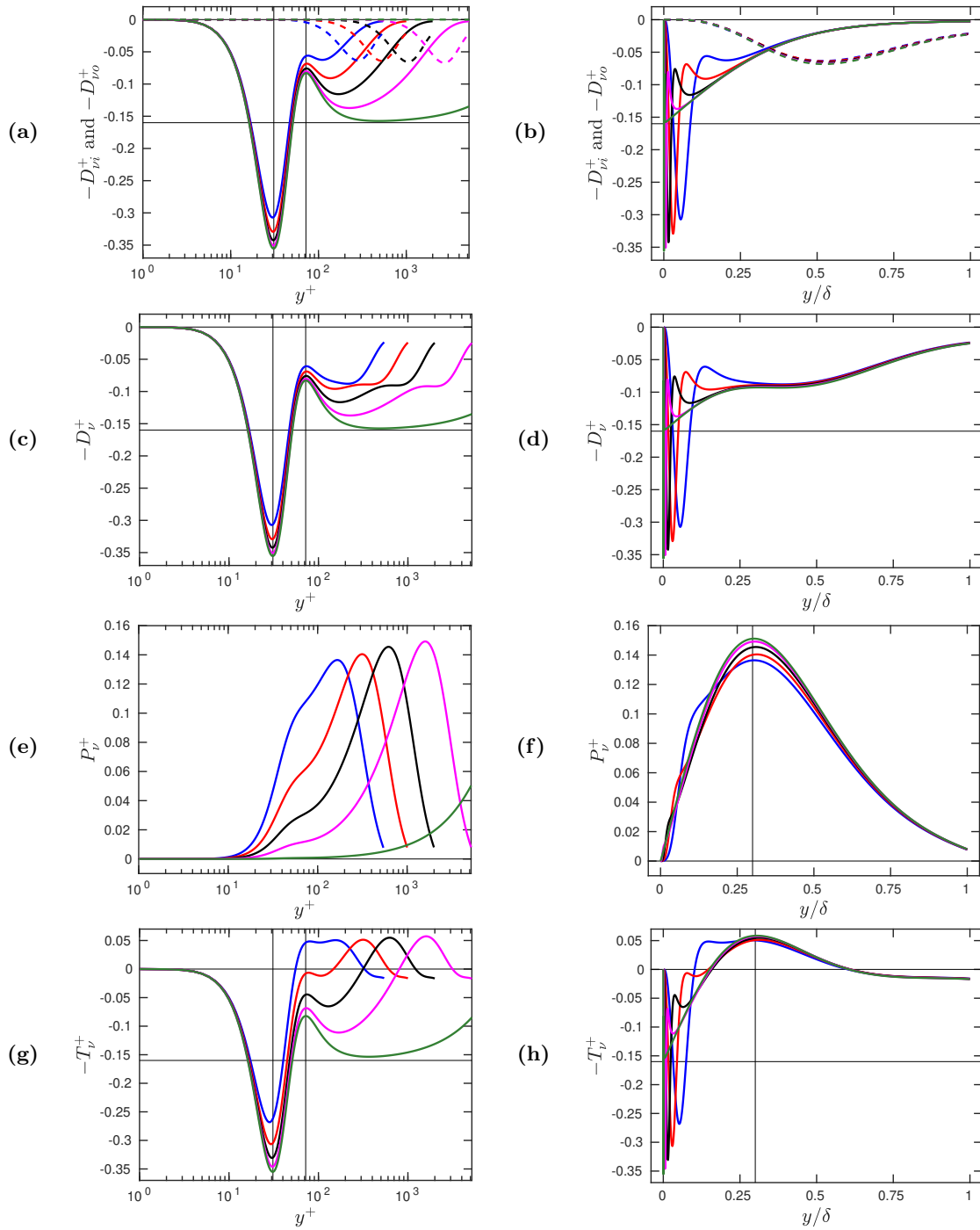


**Fig. 7** : Same as figure 6, but for pipe flows. On (f,h) the vertical lines are at  $y = 0.3\delta$ .

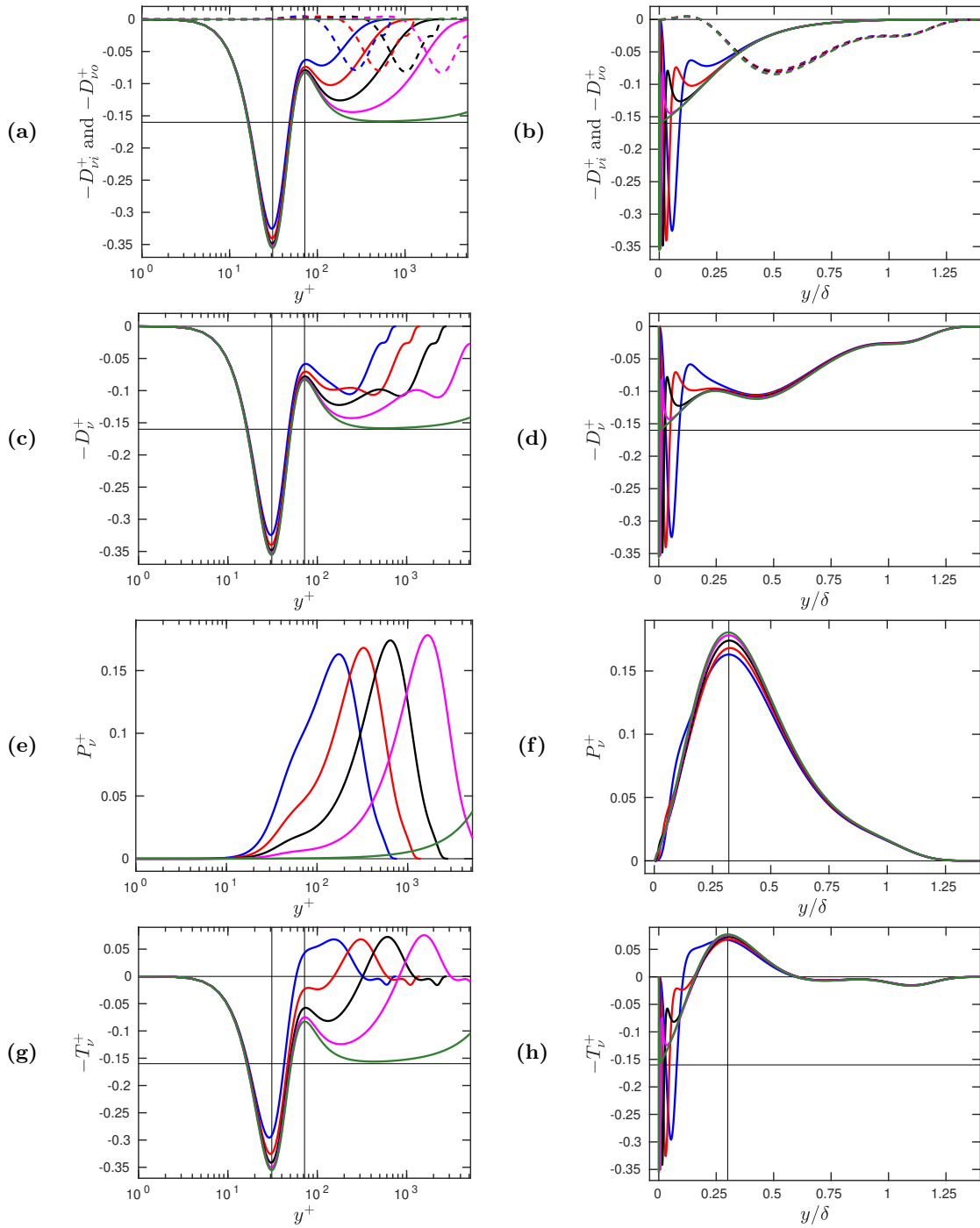


**Fig. 8** : Same as figure 6, but for boundary layers; in all graphs  $1 \leq y^+ \leq 1.4\delta^+$ . On (f) the vertical line is at  $y = 0.32\delta$ , on (h) it is at  $y = 0.3\delta$ .

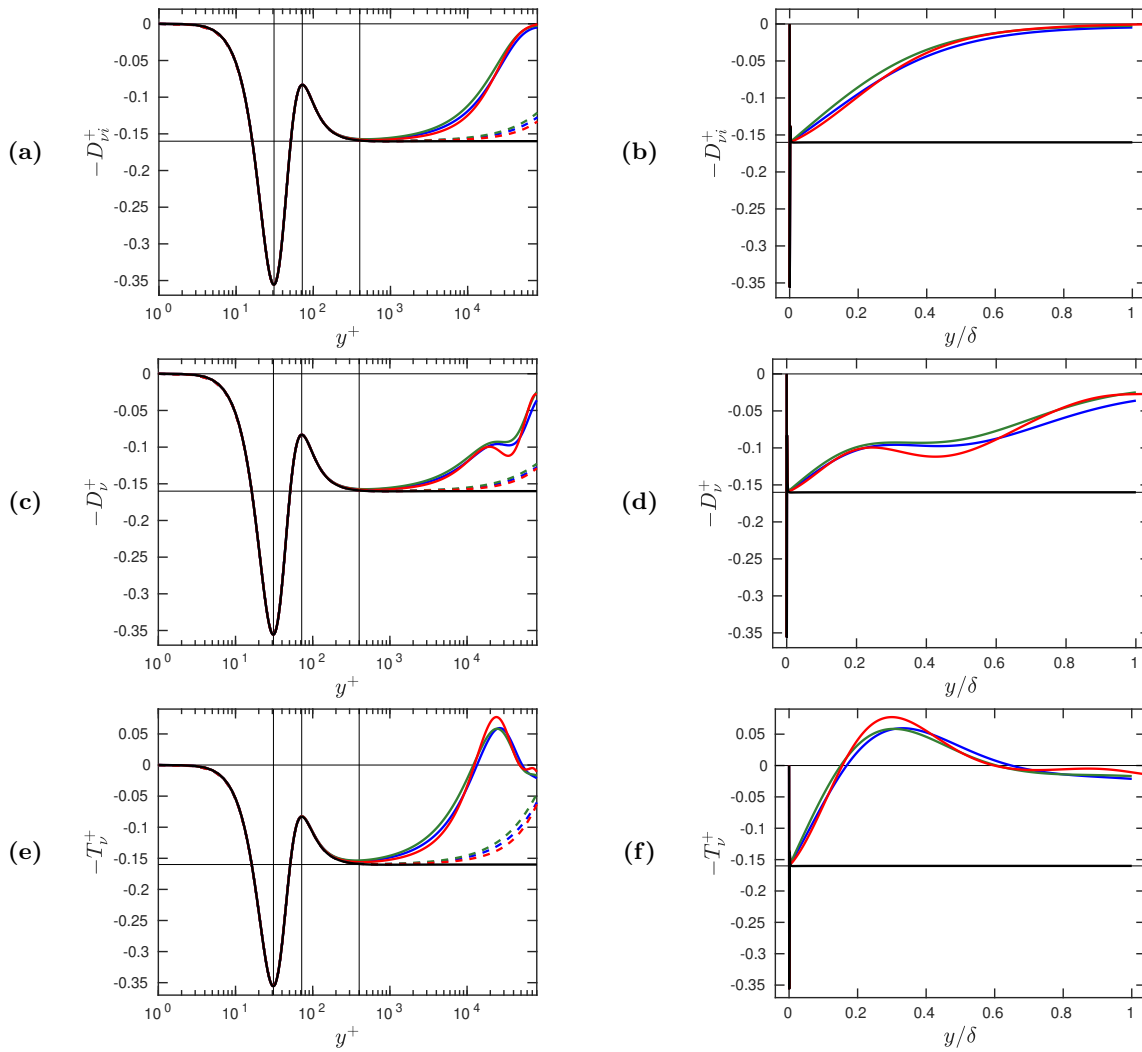


**Fig. 9** : The black curves show  $-D_{\nu ia}^+$ , see (22), calculated with  $Re_\tau = 80000$  in (b,d,f). The blue curves for channel flow, green curves for pipe flow, red curves for boundary layer show, with  $Re_\tau = 80000$ , in (a,b)  $-D_{\nu i}^+$ , (c,d)  $-D_\nu^+$ , (e,f)  $-T_\nu^+$ . On (a,c,e) the curves of  $-D_{\nu i}^+$ ,  $-D_\nu^+$  and  $-T_\nu^+$  for  $Re_\tau = 800000$  have been added with dashed lines, and the same color codes; the vertical lines are at  $y^+ = 31, 72$  and  $400$ , the horizontal lines are at  $-T_\nu^+ = 0$  and  $-\kappa^2$ .

### 3.5 Asymptotic structure of the near-wall dissipation

The figures 6acg, 7acg and 8acg show that, as  $Re_\tau \rightarrow \infty$ , the dissipation dominates the eddy-viscosity budget in the near-wall region, the near-wall dissipation scales with  $y^+$ , and it approaches a universal asymptotic profile. This profile is obtained by replacing, in the expression (9) of the eddy-viscosity, which appears at the power 2 in  $D_{\nu i}$  (17a), the wake function  $W$  by 1, since then the wake region goes to infinity in inner scaling. This yields, as a relevant approximation of  $D_{\nu i}$ , the asymptotic dissipation function

$$D_{\nu ia} = \kappa^2 \frac{\nu^2}{L_{vK}^2} \frac{(1/S_{12}^+ - 1)^2}{f^2} \quad \text{or} \quad D_{\nu ia}^+ = \kappa^2 \frac{(1/S_{12}^+ - 1)^2}{L_{vK}^{+2}} \frac{1}{f^2}. \quad (22)$$

It is universal in that it does not depend on the flow case, but only on  $S_{12}^+$ , see the equations (10), (18) and (19). Moreover  $D_{\nu ia}^+$  considered as a function of  $y^+$  also does not depend on  $Re_\tau$ . As  $y^+ \rightarrow \infty$ , since  $1/S_{12}^+ - 1$  and  $L_{vK}^+$  approach  $\kappa y^+$ , whereas  $f \rightarrow 1$ , one has  $D_{\nu ia}^+ \rightarrow \kappa^2$ , in agreement with the expression of the log-layer eddy viscosity. This is visible on the figures 9ace; more precisely,  $|D_{\nu ia}^+ - \kappa^2| < 10^{-3}$  as soon as  $y^+ \geq 400$ . The colored curves in figures 9ace confirm that, at fixed  $y^+$ ,  $D_{\nu i}$ ,  $D_\nu$  and  $T_\nu$  approach, as  $Re_\tau \rightarrow \infty$ ,  $D_{\nu ia}$ , whatever the flow case. We have not plotted the curves for  $Re_\tau = 800000$  on figures 9bdf, since they are indistinguishable, in outer scaling, from the curves for  $Re_\tau = 80000$ . From a physical point of view, these results suggest that near-wall dissipation is due to universal near-wall motions.

The differences between  $T_\nu$  and  $-D_{\nu ia}$  in the outer region, visible on the figure 9f, are due to the contribution of the production  $P_\nu$  and outer dissipation  $-D_{\nu o}$ , which are now studied in the limit  $Re_\tau \rightarrow \infty$ .

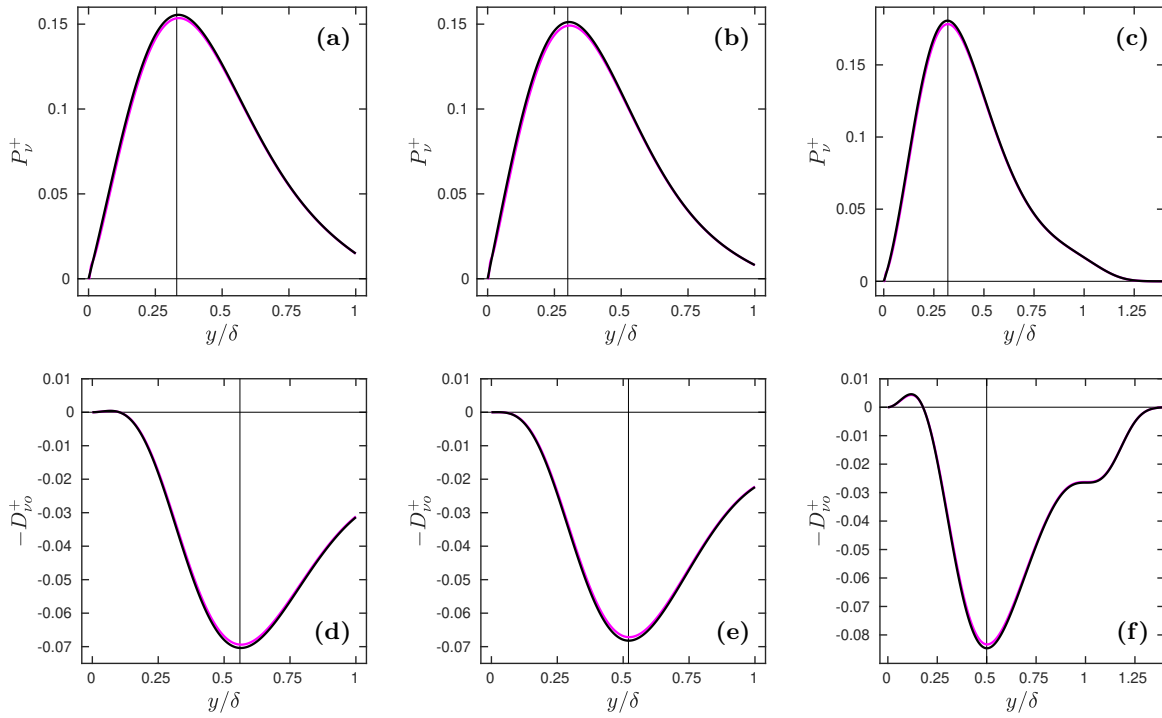


**Fig. 10** : For channel flow (a,d), pipe flow (b,e), boundary layer (c,f). The black curves show  $P_{\nu a}^+$ , see (24), the magenta curves  $P_{\nu}^+$  for  $Re_{\tau} = 5186$  in (a,b,c). The black curves show  $-D_{\nu o a}^+$ , see (26), the magenta curves  $-D_{\nu o}^+$  for  $Re_{\tau} = 5186$  in (d,e,f). The vertical lines are at  $y/\delta = 0.33$  (a),  $0.3$  (b),  $0.32$  (c),  $0.56$  (d),  $0.52$  (e),  $0.5$  (f).

### 3.6 Asymptotic structure of the production

The figures 6ef, 7ef and 8ef show that, as  $Re_{\tau} \rightarrow \infty$ , the production of the eddy viscosity vanishes in the near-wall region, scales with  $y/\delta$ , and approaches asymptotic profiles that depend only on the flow case. These profiles are obtained by replacing, in the second expression of  $P_{\nu}$  (17b), transformed in inner units,

$$P_{\nu}^+ = \kappa \frac{\nu^+}{S_{12}^+ L_{vK}^+ \delta^+} (-4W'), \quad (23)$$

the eddy viscosity  $\nu^+$ , the strain rate  $S_{12}^+$  and the von Karman length-scale  $L_{vK}^+$  by their approximations valid as  $y^+ \rightarrow \infty$ , i.e.  $\kappa y^+ W$ ,  $1/\kappa y^+$  and  $\kappa y^+$  respectively, see the discussions after equations (9-12) for  $\nu^+$  and  $S_{12}^+$ , equation (18) for  $L_{vK}^+$ . This yields the asymptotic profiles

$$P_{\nu a}^+ = \kappa^2 \frac{y}{\delta} (-4WW') \quad \text{or} \quad P_{\nu a} = \kappa^2 u_{\tau}^2 \frac{y}{\delta} (-4WW'). \quad (24)$$

The first equation shows that  $P_{\nu a}^+$  is, for a fixed flow case, a function of  $y/\delta$  only, because the wake function  $W$  depends only on  $y/\delta$ , see equations (13) and (14). The figures 10abc confirm that, at fixed  $y/\delta$ ,  $P_{\nu}^+$  approaches  $P_{\nu a}^+$  as  $Re_{\tau} \rightarrow \infty$ . For  $Re_{\tau} = 80000$ , the profiles of  $P_{\nu}^+$  for the three flow cases are indistinguishable from the corresponding functions  $P_{\nu a}^+$  at the scale of the figures 10abc. From a physical point of view, these results suggest that production is due to large-scale outer motions. The comparison between the vertical scales of the figures 10abc also suggest that these motions contribute more efficiently to the production of  $\nu_t$  in the boundary layer than in the other flows. This might be related to the fact that the boundary layer is in principle unbounded in the wall-normal direction, contrarily to channel and pipe flows.

### 3.7 Asymptotic structure of the outer dissipation

The figures 6ab, 7ab and 8ab show that, as  $Re_{\tau} \rightarrow \infty$ , the outer dissipation of the eddy viscosity vanishes in the near-wall region, scales with  $y/\delta$ , and approaches asymptotic profiles that depend only on the flow case. These profiles are obtained by starting from the second expression of  $D_{\nu o}$  (17c), transformed in inner units,

$$D_{\nu o}^+ = \frac{1}{\delta^{+2}} (1/S_{12}^+ - 1)^2 (W'^2 + WW''), \quad (25)$$

and applying one of the approximations that led from (23) to (24), i.e. replacing  $1/S_{12}^+ - 1$  by  $\kappa y^+$ . This yields the asymptotic profiles

$$D_{\nu_{oa}}^+ = \kappa^2 \left(\frac{y}{\delta}\right)^2 (W'^2 + WW'') \quad \text{or} \quad D_{\nu_{oa}} = \kappa^2 u_\tau^2 \left(\frac{y}{\delta}\right)^2 (W'^2 + WW''). \quad (26)$$

Similar to  $P_{\nu_a}^+$  (24),  $D_{\nu_{oa}}^+$  is, for a fixed flow case, a function of  $y/\delta$  only. The figures 10def confirm that, at fixed  $y/\delta$ ,  $D_{\nu_o}^+$  approaches  $D_{\nu_{oa}}^+$  as  $Re_\tau \rightarrow \infty$ . For  $Re_\tau = 80000$ , the profiles of  $D_{\nu_o}^+$  for the three flow cases are indistinguishable from the corresponding functions  $P_{\nu_a}^+$  at the scale of the figures 10def. From a physical point of view, this contribution to the dissipation is probably due to large-scale outer motions.

### 3.8 QR6 on the BL case inspired from Spalart & Allmaras (1994)

- **Q6** (Emmanuel, May 22) : Spalart & Allmaras (1994) study in their section II.3 *Near-wall region, high Re number* the ZPGTBL case. In their figure 6 they show the ‘budget of  $\nu_t$ ’, and they claim that

‘The sum (i.e.  $D\nu_t/Dt$ ) is positive throughout’.

Indeed if one states that the general  $\nu_t$  eq. has on its lhs

$$\frac{D\nu_t}{Dt} = \frac{\partial\nu_t}{\partial t} + U_i \frac{\partial\nu_t}{\partial x_i} \simeq U \frac{\partial\nu_t}{\partial x} + V \frac{\partial\nu_t}{\partial y}, \quad (27)$$

this may be **positive throughout** the BL because of the advection - the expansion of the BL or, as they write it on P12, because of the ‘**advance of the turbulent front**’...

**Does this mean that in the BL case the lhs of our  $\nu_t$  eq (15) is not 0 but a positive function of  $y$ , that we might deduce, for instance, from the DNS of Sillero *et al.* (2013) ?**

**The bad news then would be that the ‘Prandtl number’  $\sigma$  would not scale out !..**

**What do you think ?**

- **R6** (Stefan, May 28) : We calculate  $\nu_t$  from **stationary** Reynolds shear stress and shear rate. My understanding of Fig. 6 is that this is a consequence of model parameter settings: production, dissipation, ... are crudely represented in the Spalart model, see e.g. Pope last page before Chapter 11.
- **R6** (Emmanuel, June 2) : In BL **advection** may come into play, i.e. the lhs of the  $\nu_t$  equation, given by (27), could be nonzero though the mean fields are stationary.

**Should we study this, for instance, on the DNS of Sillero *et al.* (2013) ?**

**Or, could we ‘prove’, by estimating order of magnitudes, that  $D\nu_t/Dt$  is in principle ‘small’ ?**

- **R6** (Stefan, June 4) : **you want to submit in July, just forget about it! I don’t think it’s worth the time.**

## References

- ABDOL-HAMID, K. S. 2015 Assessments of  $k - kL$  Turbulence Model Based on Menter's Modification to Rotta's Two-Equation Model. *Int. J. Aerospace Engineering* **2015**, 1–18, <http://downloads.hindawi.com/journals/ijae/2015/987682.pdf>.
- BALDWIN, B. & BARTH, T. 1990 A one-equation turbulence transport model for high Reynolds number wall-bounded flows. *NASA Technical Memorandum* pp. 102847, 1–20.
- CHIN, C., MONTY, J. & OOI, A. 2014 Reynolds number effects in DNS of pipe flow and comparison with channels and boundary layers. *Int. J. Heat & Fluid Flow* **45**, 33 – 40.
- EGOROV, Y., MENTER, F., LECHNER, R. & COKLJAT, D. 2010 The scale-adaptive simulation method for unsteady turbulent flow predictions. Part 2: Application to complex flows. *Flow, Turbulence & Comb.* **85**, 139–165.
- HEINZ, S. 2018 On mean flow universality of turbulent wall flows. I. High Reynolds number flow analysis. *J. Turbulence* **19**, 929–958.
- HEINZ, S. 2019 On mean flow universality of turbulent wall flows. II. Asymptotic flow analysis. *J. Turbulence* **20**, 174–193.
- LEE, M. & MOSER, R. D. 2015 Direct numerical simulation of turbulent channel flow up to  $Re_\tau \approx 5200$ . *J. Fluid Mech.* **774**, 395–415.
- MENTER, F. & EGOROV, Y. 2006 Revisiting the turbulent scale equation. *IUTAM Symposium on One Hundred Years of Boundary Layer Research*, pp. 279–290. Springer.
- MENTER, F. R. 1997 Eddy viscosity transport equations and their relation to the  $k - \epsilon$  model. *J. Fluids Eng.* **119**, 876–884.
- MENTER, F. R. & EGOROV, Y. 2010 The scale-adaptive simulation method for unsteady turbulent flow predictions. Part 1: theory and model description. *Flow, Turbulence & Comb.* **85**, 113–138.
- NEE, V. W. & KOVASZNY, L. S. G. 1969 Simple phenomenological theory of turbulent shear flows. *Phys. Fluids* **12**, 473–484.
- SILLERO, J. A., JIMÉNEZ, J. & MOSER, R. D. 2013 One-point statistics for turbulent wall-bounded flows at Reynolds numbers up to  $\delta^+ \simeq 2000$ . *Phys. Fluids* **25**, 105102,1–16.
- SPALART, P. & ALLMARAS, S. 1994 A one-equation turbulence model for aerodynamic flows. *Recherche Aéronautique* **1**, 5–21.
- VALLIKIVI, M., HULTMARK, M. & SMITS, A. J. 2015 Turbulent boundary layer statistics at very high Reynolds number. *J. Fluid Mech.* **779**, 371–389.
- YOSHIZAWA, A., ABE, H., MATSUO, Y., FUJIWARA, H. & MIZOBUCHI, Y. 2012 A Reynolds-averaged turbulence modeling approach using three transport equations for the turbulent viscosity, kinetic energy, and dissipation rate. *Phys. Fluids* **24**, 075109.

---

## Archives: links to important previous versions

- **V0.055 of May 19, 2020:** memory of the [section 4.1 Comparison with Hamba \(2013\)](#), of [figure 9](#) for  $P_\nu$  and  $P_{\nu H}$ , of [QR5](#) regarding this comparison.
- **V0.025 of May 7, 2020:** memory of [figure 5](#) for  $W'/W$  and  $(W'^2 + WW'')/W^2$ , [QR3](#) regarding comparisons with DNS of pipe flow, [QR4](#) regarding comparisons with DNS of BL, [figure 10](#) for  $-T_\nu^+$  et al. in BL with an extended range of  $y^+$ .
- **V0.015 of April 29, 2020:** memory of [QR1](#) regarding near-wall effects / the kinematic viscosity & [QR2](#) regarding pipe flow / curvature effects.